J. Min. Metall. Sect. B-Metall. 58 (3) (2022) 439 - 450

Journal of Mining and Metallurgy, Section B: Metallurgy

MICROSTRUCTURE EVOLUTION AND MECHANICAL PROPERTIES OF TiB/Ti6Al4V COMPOSITES BASED ON SELECTIVE LASER MELTING

X. Huang [a,b,c], Y.-T. Zhu [b,c], W.-D. Huang [a,b,c,*], S.-S. Qin [b,c], L. Wang [b,c]

[a] Fujian Key Laboratory of Intelligent Machining Technology and Equipment, Fujian University of Technology, Fuzhou, China

[b] Advanced Manufacturing Productivity Promotion Center of Fujian province, Fuzhou, China

[c] Academy of Mechanical and Automotive Engineering, Fujian University of Technology, Fuzhou, China

(Received 22 April 2022; accepted 03 October 2022)

Abstract

In this paper, Ti6Al4V+3 wt.% TiB_2 composite powder was used as a raw material to synthesize TiB whiskers in situ and prepare composites reinforced with TiB/Ti6Al4V whiskers by selective laser melting (SLM). The effects of process parameters on the properties of TiB/Ti6Al4V samples were systematically studied. The evolution of the microstructure, including the formation and regulation of whiskers, and the effects on mechanical properties were discussed. The results showed that during the SLM process, adjusting the energy density effectively inhibited cracking in the TiB/Ti6Al4V samples. The TiB_2 particles acted as nucleation centers to significantly refine the grains during processing and reacted with elemental Ti to form a needle-like TiB network at the grain boundaries, which strengthened the whiskers. Additionally, TiB played a role in dispersion strengthening. Compared with Ti6Al4V, the microhardness of TiB/Ti6Al4V was 430.6±11.45 HV, an increase of 27.9%, and the wear volume of the sample was 0.85×10^{-3} mm^3, a decrease of 62.64%.

Keywords: *Selective laser melting; Ti6Al4V; TiB whisker enhancement; Mechanical properties*

1. Introduction

Selective laser melting (SLM) can produce metal parts via the use of a laser beam to perform layer-by-layer melting of metal powders according to a three-dimensional model. The advantages of SLM include high processing accuracy and efficient production, and these advantages have attracted significant attention in various fields [1-2]. Among the materials used in SLM, Ti6Al4V is widely applied in various industries such as biomedicine and aerospace due to its excellent performance [3-4]. However, the use of conventional processing technology to process titanium alloys has had limited success [5]. The utilization of SLM technology can greatly reduce machining allowances, processing, and application costs and expand the use of titanium alloys. Furthermore, due to the rapid cooling and rapid heating steps in SLM, the grains are greatly refined, and their mechanical properties are improved compared with those of as-cast titanium alloys [6-7]. However, due to the limitations of the material properties of titanium alloys, e.g., low microhardness and poor wear resistance [8], further applications of these alloys have been restricted.

Some scholars have effectively improved the overall mechanical properties of the material by adding hard ceramic particles to the titanium alloy powder [9]. Compared with TiC [10], SiC [11], ZrO_2 [12] and other ceramic particles that are directly used as reinforcing phases, adding TiB_2 particles to the titanium alloy matrix powder to synthesize short-fiber-like TiB whiskers in situ [13], which have good interfacial bond strength with the matrix material. Additionally, due to the hardness of TiB and its role as a nucleating agent during material solidification, it can significantly improve the microhardness and wear resistance of the matrix [14-15].

Considerable research has been performed regarding the addition of TiB_2 to Ti6Al4V. For example, Su Yue et al. [16] studied the processability, microstructure evolution, and mechanical properties of samples with different contents of TiB_2 and found that TiB_2 significantly improved the microhardness of TiB/Ti6Al4V composites. Cai Chao et al. [17] used SLM and TiB_2/Ti6Al4V powder to prepare TiB/Ti6Al4V samples. These investigators found that the microstructure of the samples consisted of mutually parallel band structures and contained TiB_2 aggregates that were generated in situ in some areas.

* *Corresponding author: hwd@fjut.edu.cn*

https://doi.org/10.2298/JMMB220422025H

Harshpreet Singh et al. [18] studied the effect of different TiB_2 additions on the dynamic mechanical properties of the samples and determined that the optimal addition of TiB_2 was between 2 wt.% and 5 wt.%. Furthermore, when the addition of TiB_2 exceeded 5 wt.%, the relative density of the composite increased, and the ductility of the titanium alloys was lost. However, most of these studies have focused on the addition of TiB_2 and the improvement of mechanical properties, and there has been less research on the effect of energy input on the transformation of TiB_2 to TiB and formation of cracks during processing.

Therefore, in this study, samples were prepared by SLM using Ti6Al4V powder with 3 wt.% TiB_2 and various process parameters. The effects of different process parameters on the growth of the enhanced phase at grain boundaries are discussed and quantitatively analyzed in this paper.

2. Experiments

2.1. Powder preparation

Ti6Al4V powder with an average particle size of 30 μm was selected as the matrix powder, and TiB_2 particles with an average particle size of 1 μm and a purity of 99.99% were selected as the reinforcing phase, as shown in Fig. 1(a-b). The Ti6Al4V powder and TiB_2 particles were mixed in a planetary ball mill for 4 h at 200 rpm, and the mass ratio of ball to material was 5:1. During the mixing process, the ball mill tank was maintained under argon. After mixing, the TiB_2 particles were uniformly dispersed in the Ti6Al4V powder, as shown in Fig. 1(c-d). In addition, diffraction peaks of TiB_2 and TiB were not observed in the X-ray diffraction (XRD) analysis of the composite powder, which indicated that the TiB_2 particles did not react with the Ti6Al4V powder during the mixing process.

2.2. SLM process

The SLM equipment was developed and manufactured by SLM Solutions GmbH and equipped with a continuous wave fiber laser with a maximum laser power of 400 W. Before processing, the TiB_2/Ti6Al4V mixture was dried in a vacuum oven at a temperature of 80 °C for 6 h. The substrate was processed by shot peening. During processing, the chamber was filled with argon (purity 99.99%) to

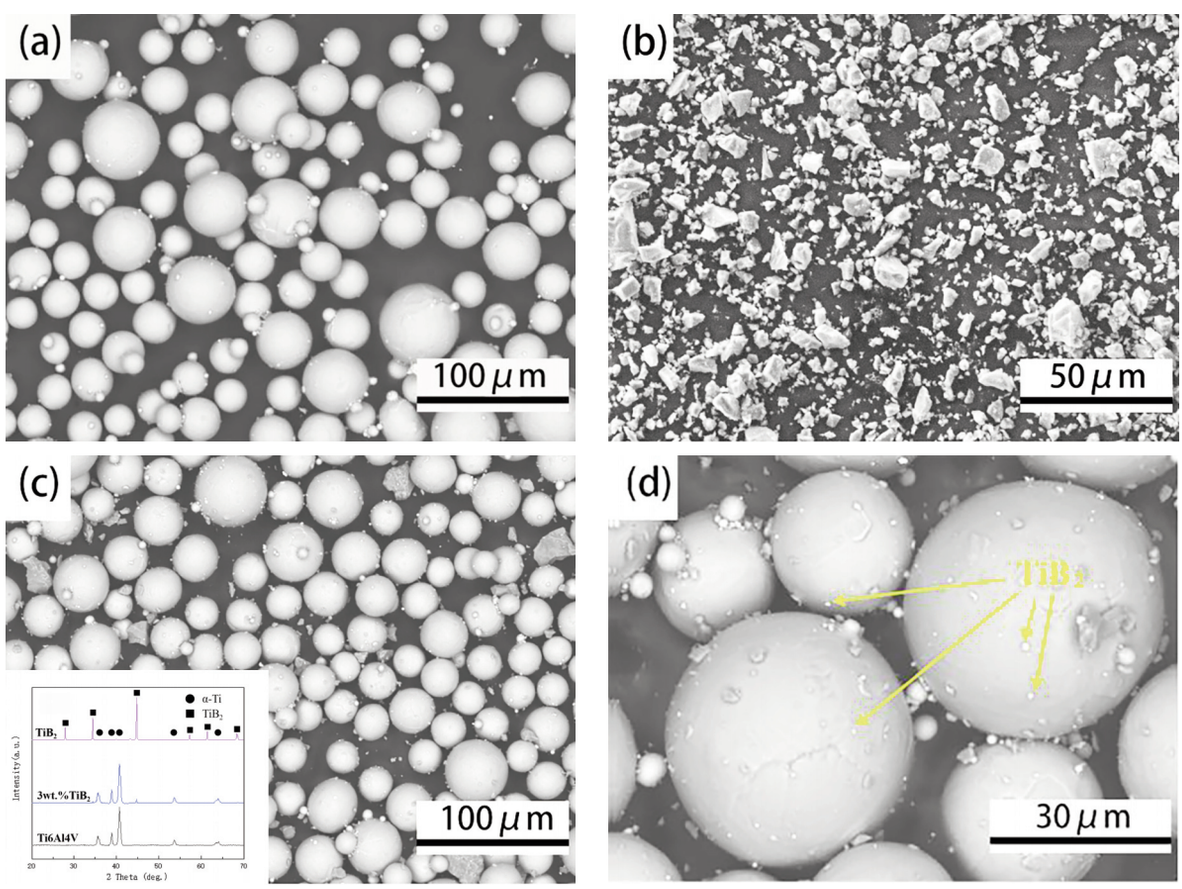

Figure 1. *Experimental raw materials. (a) Ti6Al4V; (b) TiB_2 and (c)(d) TiB_2/Ti6Al4V composite powder*

maintain the oxygen concentration below 0.1%; the substrate temperature was maintained at 200 °C.

Samples of dimensions 10×10×10 mm were manufactured by SLM for subsequent experiments. The processing of the TiB_2/Ti6Al4V composite powder involved a laser power (P) that ranged from 255 to 335 W. The laser scan speed (v) ranged from 500 to 1300 mm/s, the hatch space (h) was 0.12 mm, and the layer thickness (t) was 0.03 mm. The specific experimental parameters are shown in Table 1. In addition, 10x10x10 mm samples were manufactured using the optimal process parameters of Ti6Al4V powder provided by the equipment manufacturer.

Table 1. *Factor level table*

Experimental factor	Experimental level
Laser power (W)	255, 275, 295, 315, 335
Scan speed (mm/s)	500, 700, 900, 1100, 1300
Hatch space (mm)	0.12
Layer thickness (mm)	0.03

The energy per unit volume was represented by the energy density, which was expressed as:

$$\delta = \frac{P}{v * h * t}$$

2.3. Characterization of mechanical properties and microstructure

The samples were cleaned in absolute ethanol using sonication. After grinding and completely polishing the sample surface, vacuum drying was used to determine its relative density with a Mettler Toledo ME204E analytical balance according to the Archimedes drainage method. Additionally, the cross section of the sample was determined via a KH1300 three-dimensional microscope system. An MVA-402TS microhardness tester was used for Vickers microhardness testing; the test force was 1000 gf, and the dwell time was 20 s. The measurement was repeated 5 times; the maximum and minimum values were removed, and the average value was calculated. A high-load UMT-Tribolab scratch tester was employed for the wear resistance test. The friction pair material was a tungsten-cobalt alloy (92HRC), the load was 3 N, the friction time was 10 min, the scratch length was 5 mm, and the friction speed was 10 mm/sec. A Hitachi TM3030plus desktop scanning electron microscope was utilized for topographical analysis of wear scars. The metallographic specimens were etched using Kroll's reagent (3% HF, 6% HNO_3, 91% H_2O) and analyzed using field emission scanning electron microscopy (FESEM; FEI's Nova NanoSEM 450) and energy dispersive spectrometry (EDS; Oxford X-MaxN). The sample microstructure was characterized. The second phase was analyzed using Nano Measurer and ImageJ software.

3. Results and Discussion

3.1. Relative Density and Cracks

As shown in Fig. 2(a), the relative density of the as-prepared sample varied with the laser power and scan speed. When the scan speed was reduced and the laser power was appropriately increased, the overall relative density of the sample increased. When the laser power was 315 W and the scan speed was 500 mm/s, the maximum relative density of the sample was 97.16%; its cross section is shown in Fig. 2(b). This cross section had few pores and few unmelted particles. When the laser power was increased, overburning occurred, a large amount of molten metal evaporated to form metal vapor, and the relative density decreased. When the scan speed was too fast (1300 mm/s), the time that the laser acted on the powder was too short, and the energy input was insufficient. This made it difficult to melt TiB_2 particles with a high melting point, especially when the laser power was 255 W. Sample A exhibited many unmelted TiB_2 particles, which were clearly observed in the sample cross section, as shown in Fig. 2(c).

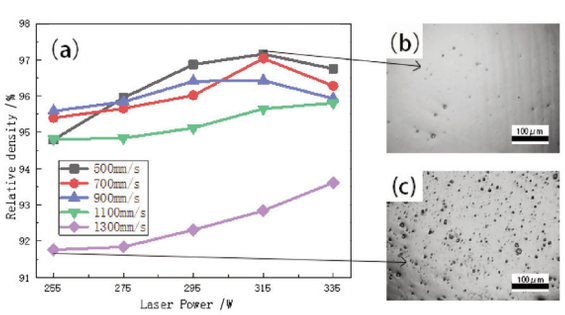

Figure 2. *(a) The variation in the relative density of TiB/Ti6Al4V composites prepared with different SLM process parameters ;(b)(c) cross sections of the samples*

The relative density of Ti6Al4V prepared by SLM was 99.2%, which was greater than the maximum density of TiB/Ti6Al4V composite samples. The TiB_2 particles clearly demonstrated weak bonding with the matrix material, which lessened the overall processability to a certain extent [19]. The boiling point of aluminum in Ti6Al4V is approximately 2519 °C, while the laser temperature during SLM processing can exceed 3000 °C, which indicates that aluminum evaporates very easily during the SLM process [16]. During the SLM process to melt more TiB_2 with a higher melting point, it is necessary to increase the energy input by means of longer laser dwell time and greater laser power. However, this

intensifies the evaporation of aluminum and reduces the density of the TiB/Ti6Al4V composite sample.

After adding TiB_2, the stress concentration, thermal expansion coefficient difference or phase transformation stress also brought about cracking. As shown in Fig. 3(a), the sample with a lower energy density had macroscopic transverse cracks perpendicular to the processing direction on its side surface. Specimens without obvious macroscopic cracks were obtained by increasing the laser power and reducing the scan speed during processing. For example, when the laser power was 315 W, the scan speed was 500 mm/s, and when the laser power was 335 W, the scan speed was 500 mm/s. This showed that increasing the energy density inhibited the formation of cracks in TiB/Ti6Al4V samples. After adding TiB_2 particles, the higher melting point made it difficult to completely melt per unit time, and unmelted particles remained on the surface of each layer. They caused stress concentrations and reduced the bonding strength between layers. Small microcracks gradually extended along the connection surface, as shown in Fig. 3(b). The increase in energy density reduced the number of unmelted particles of TiB_2 in the material and enhanced the bonding strength between layers.

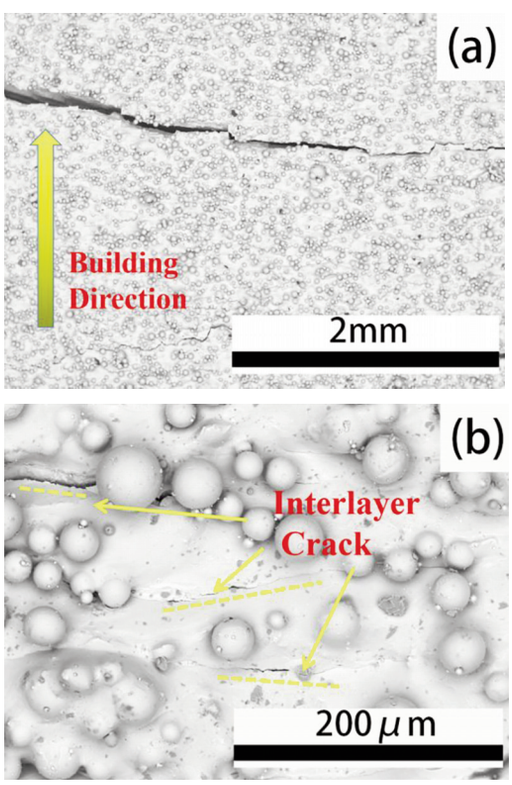

Figure 3. *SEM images of cracks. (a) Macrocracks of the samples at a laper power of 275 W and a scan speed of 900 mm/s; (b) Microcracks of the samples at a laser power of 315 W and a scan speed of 500 mm/s*

3.2. Microstructure evolution

As shown in Fig. 4(a-b), the Ti6Al4V samples prepared by SLM were dominated by needle-like α'/α martensite, while white strip-like precipitates were stacked in the TiB/Ti6Al4V samples. A clear phase boundary and a distinct network grain boundary formed.

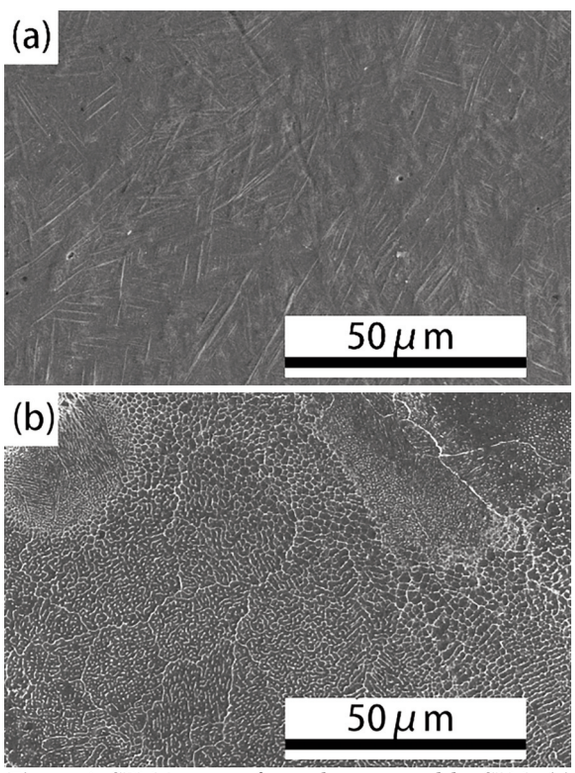

Figure 4. *SEM images of samples prepared by SLM: (a) Ti6Al4V ; (b) TiB/Ti6Al4V*

The Ti-B binary phase diagram [20], is shown in Fig. 5.

When the addition of TiB_2 to Ti6Al4V was 3 wt.%, the solidification path and phase transformation process were as follows:

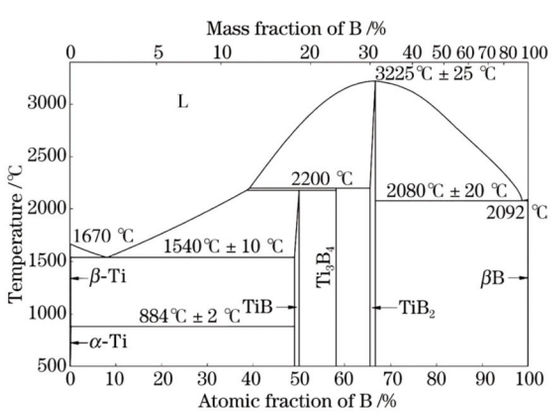

Figure 5. *Ti-B binary phase diagram [20]*

$$L \rightarrow L + TiB \rightarrow \beta - Ti + TiB \rightarrow \alpha - Ti + TiB$$

The solidification path showed that when the high-energy light source illuminated the powder, TiB_2 and Ti6Al4V began to melt, and then the TiB_2 particles reacted with the molten Ti:

$$Ti + TiB_2 \rightarrow 2TiB$$

After the laser was moved, the temperature of the molten pool decreased rapidly, TiB separated from the liquid phase, and then the liquid phase further transformed to form β-Ti and TiB. When the temperature was decreased further, β-Ti transformed into the allotrope α-Ti, but due to the rapid temperature drop, a small amount of β-Ti remained in the material. The final sample contained α-Ti, β-Ti and TiB. Due to the low solid solubility of B in the Ti matrix melt and the interaction between B and the Ti matrix, TiB precipitated at the grain boundary of the Ti matrix, and the growth rate of TiB in the [010] direction was significantly faster than that in the [100] and [001] directions [21]. Needle-like TiB whiskers were generated and aggregated in the form of whisker clusters to form a continuous network structure [22]; the evolution process is shown in Fig. 6. In addition, some of the larger TiB_2 particles remained in the sample due to the excessively fast cooling rate, as there was not enough time for them to melt, as shown in Fig. 2(c).

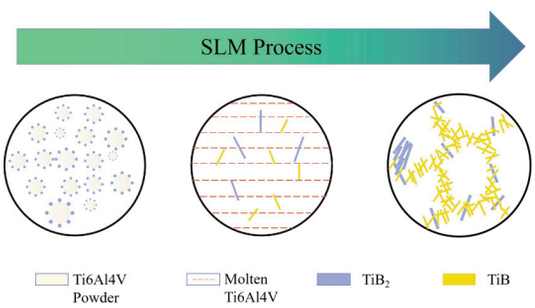

Figure 6. *Schematic illustrations of the microstructures*

To understand the phases in the samples, XRD analysis was performed on Ti6Al4V and TiB/Ti6Al4V samples prepared with different process parameters, as shown in Fig. 7. The results showed that the Ti6Al4V samples prepared by SLM were mainly composed of α/α′-Ti, and the β-Ti phase (less content) was not detected. In the TiB/Ti6Al4V samples, TiB_2 and TiB were present in addition to α/α′-Ti, which indicated that the TiB_2 particles reacted with Ti6Al4V to form TiB, although some TiB_2 remained. Specifically, when the laser power was 315 W and the scan speed was 1300 mm/s, the diffraction peak corresponding to TiB_2 was detected. By adjusting the process parameters, the scan speed was reduced to 500 mm/s, and the diffraction peaks corresponding to TiB_2 gradually became undetectable. This result indicated that the conversion of TiB_2 to

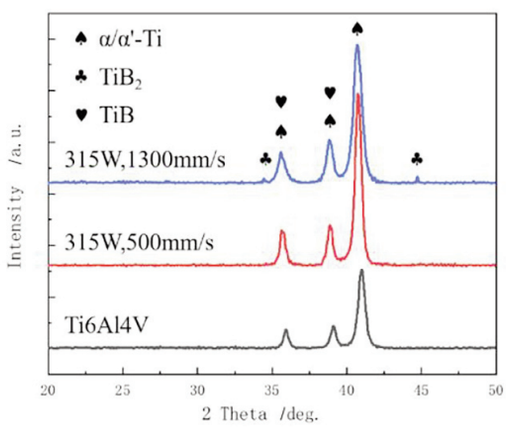

Figure 7. *XRD diffraction patterns of TiB/Ti6Al4V and Ti6Al4V samples prepared under various process parameters*

Table 2. *EDS at SEM selected locations*

Region	Element (at.%)	
	Ti	B
I	63.1	36.9
II	84.5	15.5

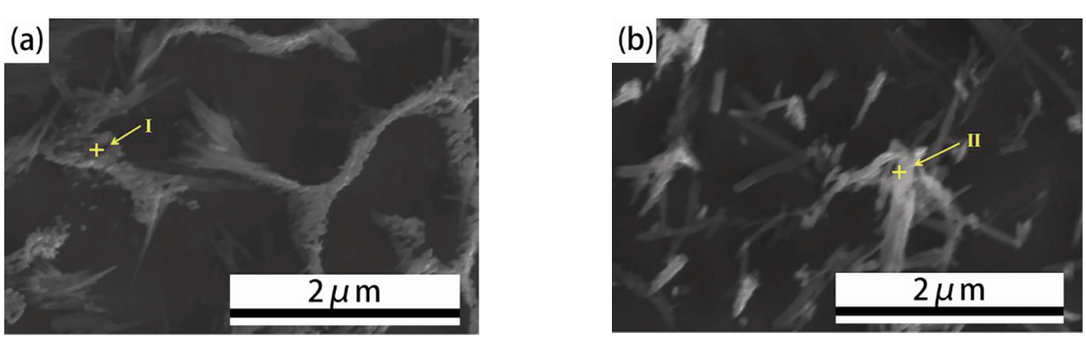

Figure 8. *TiB/Ti6Al4V samples with different process parameters. (a) laser power=315 W, scan speed=500 mm/s; (b) laser power=315 W, and scan speed=1300 mm/s*

TiB in the molten pool required a certain amount of time, and excessively fast scan speeds led to a short time of exposure of the powder to the high-energy light source, which thereby reduced the time for TiB_2 conversion.

Process parameters greatly affect the transformation of TiB_2 to TiB in Ti6Al4V [23], and the microstructures of samples prepared with different process parameters in this study are shown in Fig. 8. The EDS elemental analysis was performed on the samples, as shown in Fig. 8; the results of the analysis are shown in Table 2. The analysis showed that the proportion of B atoms at the grain boundary was affected by the process parameters. There was a higher proportion of B atoms in the samples with low-energy input and high-energy input. Due to the faster cooling rate, TiB_2 did not completely react with Ti6Al4V but remained in the newly formed grain boundary in the form of long strips [21].

To further study the variation of TiB/TiB_2, a quantitative analysis of TiB/TiB_2 (Fig. 9) was conducted; the results are shown in Fig. 10. When the scan speed was 1300 mm/s and the laser power was 315 W, the average width of TiB/TiB_2 in the sample

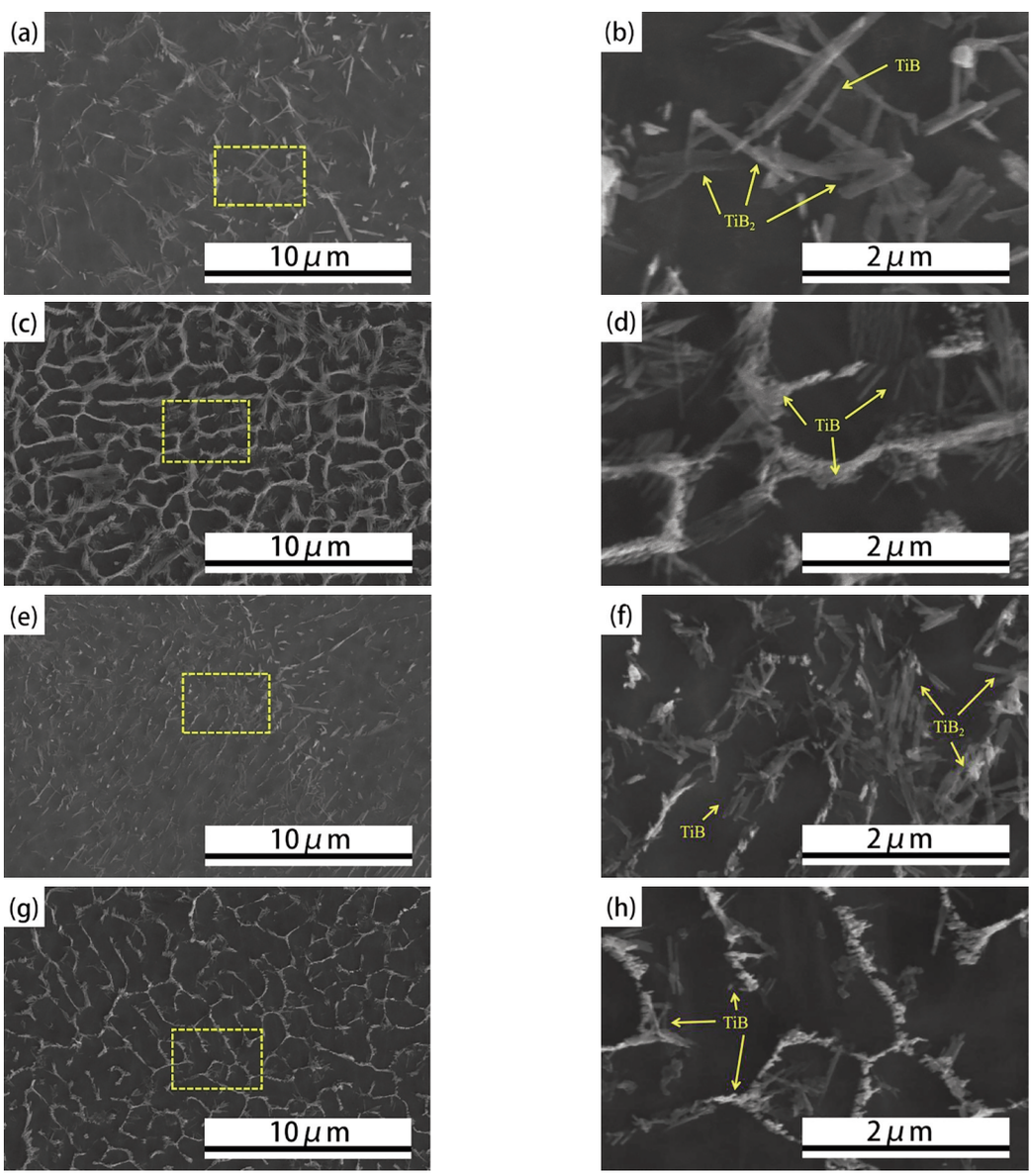

Figure 9. *SEM images of TiB/Ti6Al4V with different process parameters. (a) laser power=315 W, scan speed=1300 mm/s; (b) high resolution image of (a); (c) laser power=315 W, scan speed=500 mm/s; (d) high resolution image of (c); (e) volumetric energy density=84.60 J/mm^3; (f) high resolution image of (e); (g) volumetric energy density=163.89 J/mm^3; (h) high resolution image of (g)*

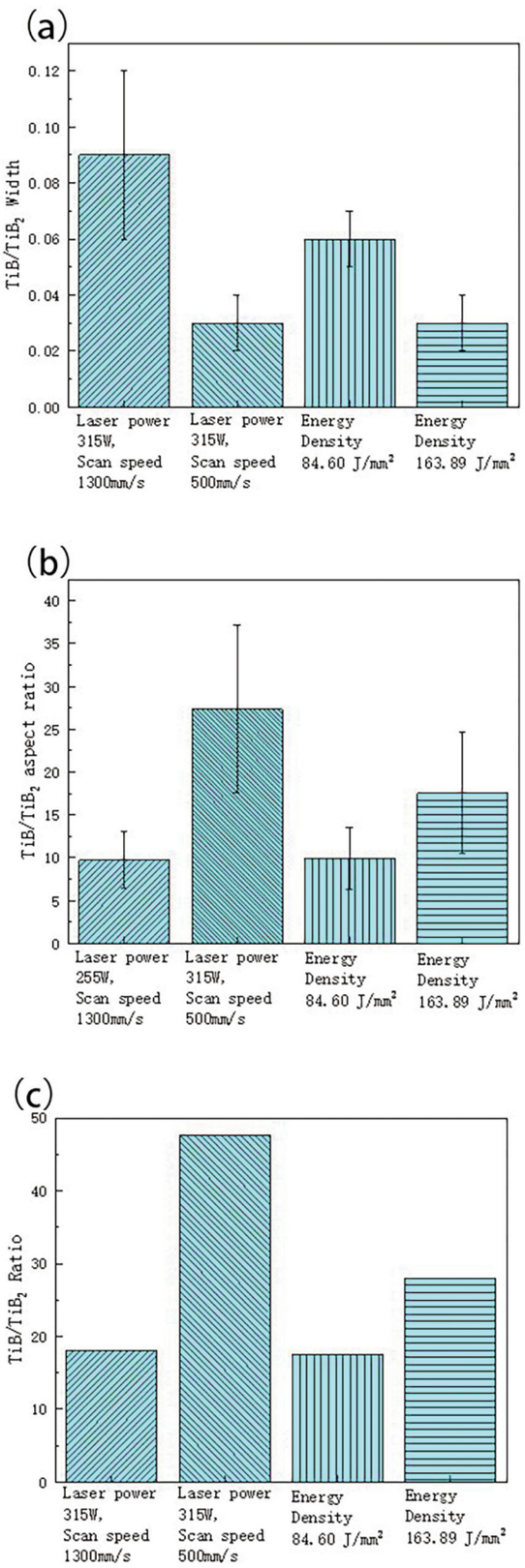

Figure 10. *(a) TiB/TiB$_2$ width, (b) TiB/TiB$_2$ aspect ratio and (c) TiB/TiB$_2$ ratio*

was 0.09±0.03 μm, and the aspect ratio was 9.76±3.32. Thus, there was a short rod-like reinforcing phase with a low aspect ratio, as shown in Fig. 9(a-b). When the scan speed was reduced to 500 mm/s, the average width of TiB/TiB$_2$ was 0.03 ± 0.01 μm, and the aspect ratio was 27.38 ± 9.78. Thus, there were needle-like reinforcing phases, as shown in Fig. 9(c–d). Combining the EDS results in Table 2 and the XRD results in Fig. 7, the short rod-like reinforcing phase was identified as TiB$_2$, while the needle-like reinforcing phase was shown to be TiB. The same behavior was observed during the process of increasing the energy density from 84.60 J/mm^3 to 163.89 J/mm^3. That is, the average width of TiB/TiB$_2$ decreased from 0.06±0.01 μm to 0.03±0.01 μm and the aspect ratio of TiB/TiB$_2$ increased from 9.91±3.60 to 17.59±7.05; its morphology is shown in Fig. 9(e–h). In the study by Jianbo Jin et al., TiB$_2$ at the grain boundary was in the form of thin rod-like hexagonal prisms, and TiB was in the shape of whiskers [24]. When the energy input was low, the energy obtained by the powder melted only Ti6Al4V with a lower melting point, and some of the TiB$_2$ did not fully react with Ti6Al4V but formed short rod-like TiB$_2$ with a low aspect ratio. By increasing the energy input during processing, the temperature of the molten pool increased, the life of the molten pool was prolonged, molten TiB$_2$ and Ti6Al4V had sufficient time to form needle-like TiB with a high aspect ratio in situ, and the generated TiB formed clusters of whiskers and accumulated at the grain boundaries. Clearly, increasing the duration and temperature of the molten pool promoted the formation of TiB. The whisker morphology changed from TiB$_2$ to TiB and increased the interfacial bonding strength between the reinforcing phase and the matrix, which suppressed the formation of cracks in the samples. In addition, the change in whisker morphology affected the grain boundaries. The proportion of TiB/TiB$_2$ was analyzed (Fig. 9(a, c, e, g)), and the results are shown in Fig. 10(c). When the laser power was 315 W and the scan speed was 500 mm/s, the proportion of TiB/TiB$_2$ reached 47.71%, and when the scan speed was adjusted to 1300 mm/s, the proportion of TiB/TiB$_2$ decreased to 18.10%. The same behavior was observed when the energy density decreased from 163.89 J/mm^3 to 84.60 J/mm^3, i.e., the proportion of TiB/TiB$_2$ decreased from 28.03% to 17.61%. Clearly, the increase in input energy promoted the transformation of TiB$_2$ to TiB, which resulted in a large amount of TiB/TiB$_2$ stacking at the grain boundaries. Additionally, the material withstood more deformation, and cracks were suppressed [25].

3.3. Microhardness

As shown in Fig. 11(a), the microhardness of the

SLM-prepared composite samples varied with laser power and scan speed. When the scan speed was between 500 mm/s and 1100 mm/s, the overall microhardness did not change much because the influence of the addition of TiB_2 particles on the microhardness was greater than that of the changes in the process parameters. When the laser scan speed was 1300 mm/s, the microhardness of the samples was less than that at the other scan speeds. Apparently, the faster scan speed prevented the powder from melting sufficiently during processing, and the results was the least microhardness. The influence of the process parameters was greater than that of the addition of TiB_2 particles. Fig. 11(a) shows that when the scan speed was 500 mm/s, the energy input was in a higher range. Due to the complete fusion and reaction of the TiB_2 particles, TiB was evenly distributed in the matrix, which had significantly greater microhardness; the measurement error was small. However, when the scan speed was 1300 mm/s, the energy input was small, and some TiB_2 particles were not melted and remained granular, which led to a decrease in the relative density of the sample. This meant that the distribution of TiB was not uniform, which resulted in larger errors in the measurement of microhardness. The same behavior was observed in the samples formed by the two sets of process parameters: scan speed = 500 mm/s, laser power = 255 W and scan speed = 500 mm/s, laser power = 275 W. The microhardness measurement error of the samples was large. Different energy inputs led to different degrees of melting of powders, especially the TiB_2 particles.

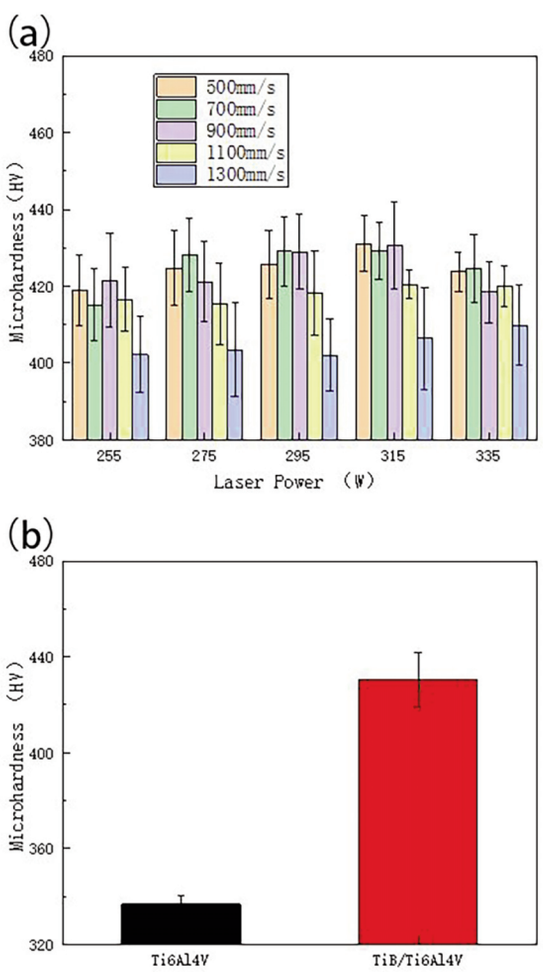

Figure 11. *(a) The variation in the hardness of TiB/Ti6Al4V composites with processed with different SLM parameters. (b) Comparison of the hardness of TiB/Ti6Al4V and Ti6Al4V*

Compared with TiB/Ti6Al4V, the microhardness of Ti6Al4V increased from 336.8±6.67 HV to 430.6±11.45 HV, an increase of approximately 27.9%, as shown in Fig. 11(b). Since the densities of TiB_2 (4.52 g/cm^3) and Ti6Al4V (4.51 g/cm^3) were similar, when the composite material was in the molten state, TiB_2 exhibited no obvious sedimentation and floating in the molten pool and was uniformly distributed throughout the whole specimen. In the samples, diffusion strengthening was evident. Additionally, TiB_2 and Ti6Al4V generated TiB in situ, and the freshly generated TiB and the remaining TiB_2 acted together as a nucleating agent to generate many refined grains and increase the total grain boundary area. The microhardness of the sample was obtained according to the Hall–Petch effect [26]. In addition, the limited dissolution of B in the Ti matrix formed an interstitial solid solution. This facilitated solid solution strengthening, increased the resistance to dislocation movement, made it difficult for slip to proceed, and increased the microhardness of the sample.

3.4. Wear resistance

To investigate the wear resistance of TiB/Ti6Al4V composites, friction and wear tests were conducted. Fig. 12(a) compares the friction coefficients of Ti6Al4V and TiB/Ti6Al4V prepared using different process parameters. The average friction coefficient of the composite material sample with a laser power of 315 W and a scan speed of 500 mm/s was 0.36, which was similar to that of the composite material sample with a laser power of 315 W and a scan speed of 1300 mm/s of 0.37. However, with increasing friction time, the friction coefficient of composite samples with faster scan speeds increased and then tended to flatten mainly due to the increase in the friction coefficient due to the contact between the friction pair and the unmelted TiB_2 particles after the wear of the base material on the surface. The average friction coefficient of Ti6Al4V was 0.42, which was higher than that of the composite samples. The wear volume of the sample decreased from 2.28×10^{-3} mm^3

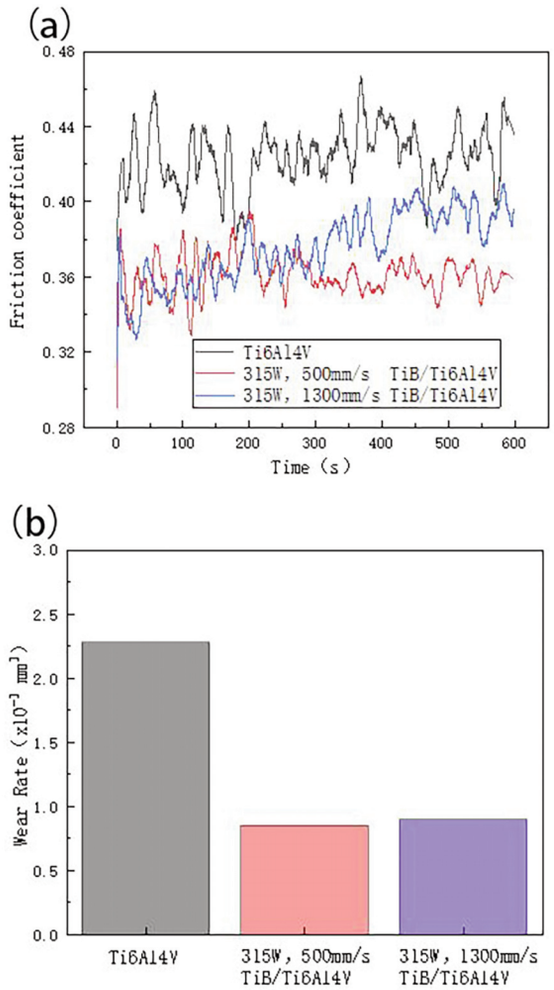

Figure 12. *Comparison of the friction properties of Ti6Al4V and TiB/Ti6Al4V prepared with different process parameters. (a) friction coefficient and (b) wear rate*

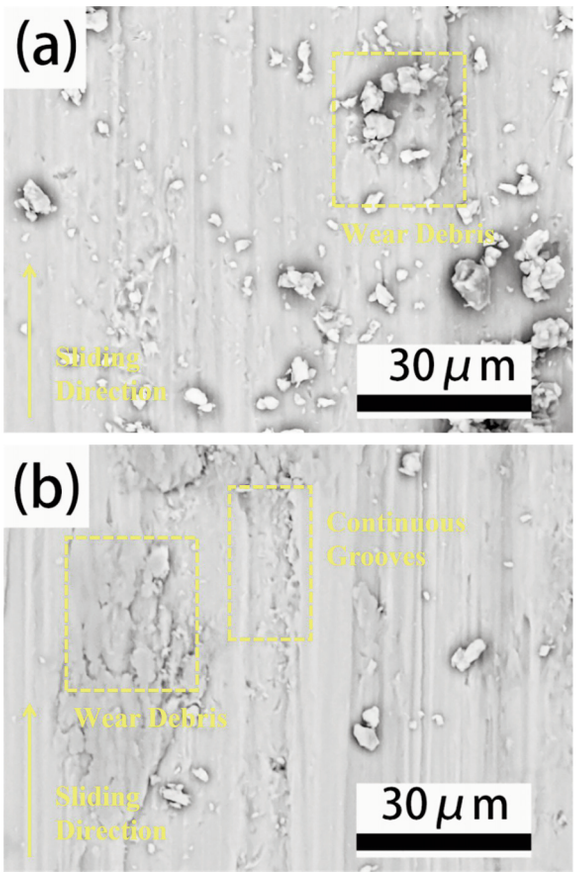

Figure 13. *SEM images of worn surfaces. (a) TiB/Ti6Al4V and (b) Ti6Al4V*

to 0.85×10^{-3} mm^3 after the addition of TiB_2 particles, which was a decrease of approximately 62.64%, as shown in Fig. 12(b). The decrease in the average friction coefficient and wear volume was attributed to the addition of TiB_2.

The worn surface morphologies of the wear scars of the TiB/Ti6Al4V and Ti6Al4V samples are shown in Fig. 13. Distinct furrows were present in all samples, but those in the TiB/Ti6Al4V samples were shallower than those in Ti6Al4V, and the worn surfaces of the TiB/Ti6Al4V samples were smoother than those of the Ti6Al4V samples. A large amount of wear debris was clearly present on the worn surface of the Ti6Al4V sample, while there was less wear debris on the worn surface of the TiB/Ti6Al4V sample. For the Ti6Al4V samples, severe plastic deformation and repeated wear behaviors occurred simultaneously during the friction process, which led to large-scale spalling on the wear surface of the samples with low microhardness; three-body wear dominated. The peeled material accumulated on the friction surface, and some of the wear debris moved with the friction pair, resulting in obvious furrows in the friction surface. For TiB/Ti6Al4V, due to the presence of the reinforcing phase, the microhardness was greater, the wear debris did not easily fall off the friction surface, and the abrasive wear mechanism changed from three-body to two-body. Therefore, the wear resistance of the TiB/Ti6Al4V samples was better than that of the Ti6Al4V samples.

4. Conclusion

In this study, experiments were performed to systematically investigate the effects of SLM process parameters on 3 wt.% TiB/Ti6Al4V composites. The following main conclusions were drawn:

1. Composite TiB/Ti6Al4V samples were prepared by SLM. When the laser power was 315 W and the scan speed was 500 mm/s, the maximum density of the sample was 97.16%. Higher energy density inhibited the formation of cracks in the samples.

2. A continuous network structure formed in the

TiB/Ti6Al4V samples prepared by SLM. By tuning the SLM process, the morphology and number of whiskers at the grain boundaries were controlled. When the laser power was 315 W and the scan speed was 500 mm/s, the aspect ratio of TiB/TiB_2 whiskers generated in situ reached 27.38±9.78, and their proportion reached 47.71%.

3. Dispersion, grain refinement and solid solution effects strengthened TiB/Ti6Al4V and increased its microhardness to 430.6±11.45 HV, which was 27.9% greater than that of Ti6Al4V (336.8±6.67 HV). The wear volume of TiB/Ti6Al4V (0.85×10^{-3} mm^3) was approximately 62.64% that of Ti6Al4V (2.27×10^{-3} mm^3).

Acknowledgements

This work was supported by Fund of Fuzhou Municipal Science and Technology Plan Project (No.2020-Z-10); Fujian Innovation Center of Additive Manufacturing (No.ZCZZ202-04); Fujian Provincial Department of science and technology (No.2020H6018). The authors would like to appreciate Mr. Y.X.Hou for his help in SEM observation and XRD analysis.

Author Contributions

Xu Huang: Conceptualization, Supervision, Methodology, Writing-review & editing, Yitao Zhu: Conceptualization, Writing-Original draft preparation, Investigation, Methodology, Data curation, Weidong Huang: Supervision, Methodology, Funding acquisition, Resources, Shuaishuai Qin: Writing- Reviewing and Editing, Lu Wang: Data curation.

Data Availability Statement

No additional data

Declaration of Interest Statement

The authors declare that we have no known competing financial interests or personal relationships that could have appeared to influence the work reported in this paper.

References

[1] W. Huang, X. Chen, X. Huang, H. Wang, Y. Zhu, Anisotropic study of Ti6Al4V alloy formed by selective laser melting, The Journal of The Minerals, Metals & Materials Society, 73(2021) 3804–3811. https://doi.org/10.1007/s11837-021-04765-0.

[2] J.-W. Wang, D.-Y. He, X. Wu, X.-Y. Guo, Z. Tan, Z. Zhou, W. Shao, Characterization of pre-alloyed NiTi powders produced by electrode induction-melting inert gas atomization for additive manufacturing, Journal of Mining and Metallurgy, Section B: Metallurgy, 58(2) (2022) 219-228. https://doi.org/10.2298/JMMB211019006W.

[3] D. Gu, H. Zhang, H. Chen, H. Zhang, L. Xi, Laser additive manufacturing of high-performance metallic aerospace components, Chinese Journal of Lasers, 47(05) (2020) 32-55 (in Chinese). https://doi.org/10.3788/CJL202047.0500002.

[4] W. Huang, D. He, H. Wang, S. Qin, L. Wang, X. Xu, The effect of heat treatment on the anisotropy of Ti-6Al-4V by selective laser melting, The Journal of The Minerals, Metals & Materials Society, 74(2022) 2724–2732. https://doi.org/10.1007/s11837-022-05212-4

[5] L. Shaomin, Z. Deyuan, L. Chunjian, S. Zhenyu, R. Liangliang, Influence of dynamic angles and cutting strain on chip morphology and cutting forces during titanium alloy Ti-6Al-4V vibration-assisted drilling, Journal of Materials Processing Technology, 288 (2021) 116898. https://doi.org/10.1016/j.jmatprotec.2020.116898.

[6] Q. Zhang, B. Duan, Z. Zhang, J. Wang, C. Si, Effect of ultrasonic shot peening on microstructure evolution and corrosion resistance of selective laser melted Ti–6Al–4V alloy, Journal of Materials Research and Technology, 11(2021) 1090-1099. https://doi.org/10.1016/j.jmrt.2021.01.091.

[7] K.S. Al-Rubaie, S. Melotti, A. Rabelo, J.M. Paiva, M. A. Elbestawi, S.C. Veldhuis, Machinability of SLM-produced Ti6Al4V titanium alloy parts, Journal of Manufacturing Processes, 57(2020) 768-786. https://doi.org/10.1016/j.jmapro.2020.07.035.

[8] X. Gao, J. Xu, Q. Zhou, X. Qian, M. Zhang, Effect of processing parameters on Ti6Al4V-10%B4C composite material prepared using selective laser melting, Chinese Journal of Lasers, 48(14) (2021) 126-134. https://doi.org/10.3788/CJL202148.1402012.

[9] K. Huang, W. Chen, M. Wu, J. Wang, K. Jiang, J. Liu, Microstructure and densification of the Ti6Al4V–70%TiB2 metal-ceramic by coupled multi-physical fields-activated sintering, Journal of Alloys and Compounds,820(2020)768-786. https://doi.org/10.1016/j.jallcom.2019.153091.

[10] W. Wei, Q. Zhang, W. Wu, H. Cao, J. Shen, S. Fan, X. Duan, Agglomeration-free nanoscale TiC reinforced titanium matrix composites achieved by in-situ laser additive manufacturing, Scripta Materialia, 187 (2020) 310-316. https://doi.org/10.1016/j.scriptamat.2020.06.057.

[11] F.M. Kgoete, A.P.I. Popoola, O.S.I. Fayomi,Oxidation resistance of spark plasma sintered Ti6Al4V-TiN composites, Journal of Alloys and Compounds,772(2019)943-948. https://doi.org/10.1016/j.jallcom.2018.09.106.

[12] A. Hattal, T. Chauveau, M. Djemai, J.J. Fouchet, B. Bacroix, G. Dirras, Effect of nano-yttria stabilized zirconia addition on the microstructure and mechanical properties of Ti6Al4V parts manufactured by selective laser melting, Materials & Design, 180 (2019) 107909. https://doi.org/10.1016/j.matdes.2019.107909.

[13] K. Huang, B. Li, W. Chen, J. Wang, Q. Huang, M. Wu, Y. Tian, J. Liu, Forming of the Ti6Al4V-60 %TiB2 metal-ceramic microcomponent under coupled multi-physical fields for improved microstructures and mechanical performances, Journal of Manufacturing Processes, 57 (2020) 654-667.

https://doi.org/10.1016/j.jmapro.2020.07.009.

[14] D.-W. Tan, Z.-W. Chen, W.-X. Wei, B.-C. Song, W.-M. Guo, H.-T. Lin, C.-Y. Wang, Wear behavior and mechanism of TiB2-based ceramic inserts in high-speed cutting of Ti6Al4V alloy, Ceramics International, 46 (2020) 8135-8144. https://doi.org/10.1016/j.ceramint.2019.12.041.

[15] H. Shafyei, M. Salehi, A. Bahrami, Fabrication, microstructural characterization and mechanical properties evaluation of Ti/TiB/TiB2 composite coatings deposited on Ti6Al4V alloy by electro-spark deposition method, Ceramics International, 46 (2020) 15276-15284. https://doi.org/10.1016/j.ceramint.2020.03.068.

[16] Y. Su, S.-C. Luo, L. Meng, G. Piao, W.Z. Min, Selective laser melting of in situ TiB/Ti6Al4V composites: formability, microstructure evolution and mechanical performance, Acta Metallurgica Sinica (English Letters), 33 (2020) 774-788. https://doi.org/10.1016/j.compositesb.2020.108567.

[17] C. Cai, C. Radoslaw, J. Zhang, Q. Yan, S. Wen, B. Song, Y. Shi, In-situ preparation and formation of TiB/Ti-6Al-4V nanocomposite via laser additive manufacturing: Microstructure evolution and tribological behavior, Powder Technology, 342 (2019) 73-84. https://doi.org/10.1016/j.powtec.2018.09.088.

[18] H. Singh, M. Hayat, H. Zhang, R. Das, P. Cao, Effect of TiB2 content on microstructure and properties of in situ Ti–TiB composites, International Journal of Minerals Metallurgy and Materials, 26(07) (2019) 915-924. https://doi.org/10.1007/s12613-019-1797-6.

[19] Z. Zhou, Y. Liu, X. Liu, Q. Zhan, K. Wang, Microstructure evolution and mechanical properties of in-situ Ti6Al4V–TiB composites manufactured by selective laser melting, Composites Part B: Engineering, 207 (2021) 108567. https://doi.org/10.1016/j.compositesb.2020.108567.

[20] L. Qin, J. Men, S. Zhao, G. Yang, X. Wang, Effect of TiB2 content on microstructure and mechanical properties of TiB/Ti-6Al-4V composites formed by selective laser melting, Chinese Journal of Lasers, 48(06) (2021) 55-64. https://doi.org/10.3788/CJL202148.0602102.

[21] I. Sen, S. Tamirisakandala, D.B. Miracle, U. Ramamurty, Microstructural effects on the mechanical behavior of B-modified Ti-6Al-4V alloys, Acta Materialia, 55 (2007) 4983–4993. https://doi.org/10.1016/j.actamat.2007.05.009.

[22] K. Morsi, V. V. Patel, Processing and properties of titanium–titanium boride (TiBw) matrix composites—a review, Journal of Materials Science，42 (2007) 2037-2047. https://doi.org/10.1007/s10853-006-0776-2.

[23] M. Dada, P. Popoola, N. Mathe, S. Adeosun, S. Pityana, Investigating the elastic modulus and hardness properties of a high entropy alloy coating using nanoindentation, International Journal of Lightweight Materials and Manufacture, 4 (2021) 339-345. https://doi.org/10.1016/j.ijlmm.2021.04.002.

[24] J. Jin, S. Zhou, Y. Zhao, Q. Zhang, X. Wang, W. Li, D. Chen, L.-C. Zhang, Refined microstructure and enhanced wear resistance of titanium matrix composites produced by selective laser melting, Optics & Laser Technology, 134 (2021) 106644. https://doi.org/10.1016/j.optlastec.2020.106644.

[25] L.J. Huang, S. Wang, Y.S. Dong, Y.Z. Zhang, F. Pan, L. Geng, H.X. Peng, Tailoring a novel network reinforcement architecture exploiting superior tensile properties of in situ TiBw/Ti composites, Materials Science and Engineering: A, 545 (2012) 187-193. https://doi.org/10.1016/j.msea.2012.03.019..

[26] D. Sethurama, R. Keshavamurthy, S. Paljor, P.E. Rohit, P.G. Koppad, Effect of multiple reinforcements (CNT/Si3N4) on hardness, electrical conductivity and friction coefficient of aluminium hybrid composites, Journal of Physics: Conference Series, 1455(1) (2020) 012011. https://doi.org/10.1088/1742-6596/1455/1/012011.

RAZVOJ MIKROSTRUKTURE I MEHANIČKA SVOJSTVA TiB/Ti6A14V KOMPOZITA DOBIJENIH SELEKTIVNIM LASERSKIM TOPLJENJEM

X. Huang [a,b,c], Y.-T. Zhu [b,c], W.-D. Huang [a,b,c,*], S.-S. Qin [b,c], L. Wang [b,c]

[a] Glavna laboratorija za mašinsku tehnologiju i opremu u Fuđenu, Tehnološki univerzitet u Fuđenu, Fudžou, Kina

[b] Centar za unapređenje proizvodne produktivnosti u provinciji Fuđen, Fudžou, Kina

[c] Fakultet za mašinsko i automobilsko inženjerstvo, Tehnološki univerzitet u Fuđenu, Fudžou, Kina

Apstrakt

U ovom radu korišćen je Ti6Al4V+3 wt.% TiB_2 kompozitni prah kao sirovina za sintezu TiB u obliku viskera in situ, kao i pripremu kompozita ojačanih TiB/Ti6A14V viskerima putem selektivnog laserskog topljenja (SLM). Sistematski su proučavani uticaji parametara procesa na svojsta uzoraka TiB/Ti6A14V. Diskutovano je o promeni mikrostrukture, uključujući formiranje i regulaciju viskera, kao i o uticaju na mehanička svojstva. Rezultati su pokazali da je tokom SLM procesa podešavanje gustine energije uspešno inhibiralo pucanje kod uzoraka TiB/Ti6Al4V. Čestice TiB_2 su delovale kao centri za nukleaciju koje su značajno rafinisale zrna tokom obrade i reagovale sa elementarnim Ti kako bi formirale igličastu TiB mrežu na granicama zrna što je ojačalo viskere. Pored toga, TiB je doprineo disperzionom ojačanju. U poređenju sa Ti6Al4V, mikrotvrdoća TiB/Ti6A14V uzoraka je iznosila 430.6±11.45 HV, što je predstavljalo povećanje od 27,9%, a stepen habanja uzoraka je iznosio 0.85×10^{-3} mm^3, što je predstavljalo smanjenje od 62,64%.

Ključne reči: *Selektivno lasersko topljenje; Ti6Al4V; Povećanje TiB viskersa; Mehanička svojstva*